STRUCTURAL BIOLOGY COMMUNICATIONS

ISSN 2053-230X

Received 19 October 2017
Accepted 12 December 2017

Edited by J. Newman, Bio21 Collaborative Crystallisation Centre, Australia

Keywords: disulfide catalysis; DsbD; *Neisseria meningitidis*; membrane proteins.

Production, biophysical characterization and initial crystallization studies of the N- and C-terminal domains of DsbD, an essential enzyme in *Neisseria meningitidis*

Roxanne P. Smith,[a] Andrew E. Whitten,[b] Jason J. Paxman,[a] Charlene M. Kahler,[c] Martin J. Scanlon[d] and Begoña Heras[a]*

[a]Department of Biochemistry and Genetics, La Trobe Institute for Molecular Science, La Trobe University, Bundoora, Victoria 3086, Australia, [b]Australian Centre for Neutron Scattering, Australian Nuclear Science and Technology Organisation, New South Wales 2234, Australia, [c]School of Pathology and Laboratory Medicine, The University of Western Australia, Crawley, Western Australia 6009, Australia, and [d]Medicinal Chemistry, Monash Institute of Pharmaceutical Sciences, Monash University, Parkville, Victoria 3052, Australia. *Correspondence e-mail: b.heras@latrobe.edu.au

The membrane protein DsbD is a reductase that acts as an electron hub, translocating reducing equivalents from cytoplasmic thioredoxin to a number of periplasmic substrates involved in oxidative protein folding, cytochrome *c* maturation and oxidative stress defence. DsbD is a multi-domain protein consisting of a transmembrane domain (t-DsbD) flanked by two periplasmic domains (n-DsbD and c-DsbD). Previous studies have shown that DsbD is required for the survival of the obligate human pathogen *Neisseria meningitidis*. To help understand the structural and functional aspects of *N. meningitidis* DsbD, the two periplasmic domains which are required for electron transfer are being studied. Here, the expression, purification and biophysical properties of n-*Nm*DsbD and c-*Nm*DsbD are described. The crystallization and crystallographic analysis of n-*Nm*DsbD and c-*Nm*DsbD are also described in both redox states, which differ only in the presence or absence of a disulfide bond but which crystallized in completely different conditions. Crystals of n-*Nm*DsbD$_{Ox}$, n-*Nm*DsbD$_{Red}$, c-*Nm*DsbD$_{Ox}$ and c-*Nm*DsbD$_{Red}$ diffracted to 2.3, 1.6, 2.3 and 1.7 Å resolution and belonged to space groups $P2_13$, $P321$, $P4_1$ and $P12_11$, respectively.

1. Introduction

In bacteria, disulfide-bond formation occurs in the periplasm and is mediated by the disulfide-bond (Dsb) family of proteins (Heras *et al.*, 2007, 2009; Kadokura & Beckwith, 2010). In most Gammaproteobacteria, Dsb proteins form a two-pathway system. In the oxidation pathway, DsbA and its cognate oxidase DsbB introduce disulfide bonds into newly translocated proteins that are undergoing oxidative folding in the periplasm (Kamitani *et al.*, 1992; Bardwell *et al.*, 1993; Missiakas *et al.*, 1993; Depuydt *et al.*, 2011). The isomerase pathway is composed of the isomerase DsbC and the reductase DsbD, which are responsible for reshuffling non-native disulfide bonds formed by the DsbA/DsbB system (Cho & Collet, 2013; Missiakas *et al.*, 1994, 1995; Rietsch *et al.*, 1996).

DsbD is a 59 kDa integral membrane reductase that transfers electrons from the cytoplasm to periplasmic substrate proteins (Arts *et al.*, 2015; Cho & Collet, 2013; Rietsch *et al.*, 1997). *Escherichia coli* DsbD (*Ec*DsbD) consists of a membrane-spanning domain, t-DsbD, flanked by two periplasmic domains, n-DsbD and c-DsbD (Katzen *et al.*, 2002; Cho *et al.*, 2007). The N- and C-terminal domains of DsbD

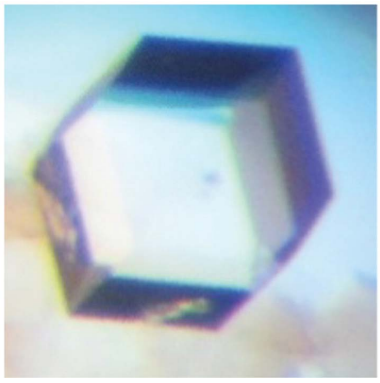

Table 1
Macromolecule-production information.

	n-*Nm*DsbD	c-*Nm*DsbD
Source organism	*N. meningitidis* strain NMB	*N. meningitidis* strain NMB
DNA source	*N. meningitidis* strain NMB	*N. meningitidis* strain NMB
Forward primer (5′–3′)	TACTTCCAATCCAATGCGAACGATCTGCTGCCGC	TACTTCCAATCCAATGCGATGTTTGCCGATACTGCCGCGC
Reverse primer (5′–3′)	TTATCCACTTCCAATGTCAGGTTTGCGGATGGTAAGTGC	TTATCCACTTCCAATGTCAGCGGTTTTGTTCATACCACTCG
Cloning vector	pMCSG7	pMCSG7
Expression vector	pMCSG7	pMCSG7
Expression host	*E. coli* BL21 (DE3) pLysS	*E. coli* BL21 (DE3) pLysS
Complete amino-acid sequence of the construct produced	MHHHHHHSSGVDLGTENLYFQSNANDLLPPEKAFVPELAVADD GVNVRFRIADGYYMYQAKIVGKTDPADLLGQPSFSKGEEKE DEFFGRQTVYHHEAQVAFPYAKAVGEPYKLVLTYQGCAEVG VCYPPVDTEFDISGNGTYHPQT	MHHHHHHSSGVDLGTENLYFQSNAMFADTAALKAAMDTALKEH PDKPVVLDFYADWCISCKEMAAYTLNQPEVHQAVDMERFFQ IDVTANKPEHQALLKEYGLFGPPGVFVVRSDGSRSEPLLGF VKADKFIEWYEQN

adopt an immunoglobulin-like and a thioredoxin-like fold, respectively (Rozhkova *et al.*, 2004). t-DsbD is membrane-embedded and consists of eight α-helices (Cho & Beckwith, 2009). Each DsbD module harbours two catalytic cysteines, which allow efficient electron flow through the three DsbD domains *via* a sequential cascade of thiol–disulfide exchange reactions (Stewart *et al.*, 1999; Katzen & Beckwith, 2000). This process begins with oxidized t-DsbD, which accepts electrons from reduced cytoplasmic thioredoxin, leaving t-DsbD reduced and thioredoxin oxidized (Stewart *et al.*, 1999). Reduced t-DsbD undergoes a conformational change which allows interaction with and reduction of c-DsbD (Cho & Collet, 2013). The latter domain reduces n-DsbD, which then reduces disulfides in its periplasmic substrates (Arts *et al.*, 2015) such as DsbC, CcmG and DsbG (Stirnimann *et al.*, 2005; Depuydt *et al.*, 2009).

Dsb proteins promote multiple virulence phenotypes and regulate the redox balance in the cell envelope, but in general these proteins are not required for survival. However, this is not the case in *Neisseria meningitidis*, where DsbD (*Nm*DsbD) was found to be essential for the viability of this obligate human pathogen (Kumar *et al.*, 2011). We are interested in investigating the structural and functional characteristics of *Nm*DsbD in order to understand the molecular basis of this uncommon phenotype. Furthermore, this information could form the basis for the future development of antineisserial agents targeting DsbD (Smith *et al.*, 2016). Here, we report the expression, biophysical characterization, crystallization and preliminary X-ray diffraction data for the two periplasmic domains of *Nm*DsbD in both redox states.

2. Materials and methods

2.1. Macromolecular production

For the expression of the N- and C-terminal domains of *Nm*DsbD (residues 1–124 and 465–579, respectively, of the mature protein), the corresponding coding regions were PCR-amplified from *N. meningitidis* strain NMB genomic DNA. Ligation-independent cloning (LIC) was then used to insert the sequences into bacterial expression vector pMCSG7 (Eschenfeldt *et al.*, 2009). The final constructs contained an N-terminal His_6 tag that preceded a *Tobacco etch virus* (TEV) protease cleavage site. This tag is used in the purification of the proteins and is cleaved during the process, leaving two additional residues (SN) on n-*Nm*DsbD and three additional residues (SNA) on c-*Nm*DsbD (Table 1).

Plasmid constructs pMCSG7::*n-NmdsbD* and pMCSG7::*c-NmdsbD* were transformed into *E. coli* BL21 (DE3) pLysS cells. n-*Nm*DsbD and c-*Nm*DsbD were expressed using the autoinduction method (Studier, 2005). Briefly, *E. coli* BL21 (DE3) pLysS cells harbouring n-*Nm*DsbD- and c-*Nm*DsbD-containing plasmids were grown at 303 K for 24 h with agitation at 180 rev min^{-1} in rich (ZY) medium supplemented with 100 µg ml^{-1} ampicillin and 34 µg ml^{-1} chloramphenicol (typically to a final optical density at 600 nm in the range between 4 and 5). Bacterial cultures were harvested by centrifugation (7500*g*, 20 min, 277 K) and flash-frozen before storage at 183 K.

For purification, harvested pellets were resuspended in 25 m*M* Tris pH 8.0, 150 m*M* NaCl supplemented with EDTA-free protease-inhibitor cocktail tablets and 400 units of DNase I per litre of culture. Cells were lysed using a bench-top cell disruptor (one cycle at 241 MPa; TS series, Constant Systems Ltd). Cellular debris was removed from the lysate *via* centrifugation (30 000*g*, 20 min, 277 K) and the lysate was loaded onto a 5 ml HisTrap FF column (GE Healthcare). Proteins were eluted from the column in 25 m*M* Tris pH 8.0, 150 m*M* NaCl and a gradient of 0–500 m*M* imidazole using a Bio-Rad NGC system. Recombinant His-tagged TEV protease (Cabrita *et al.*, 2007) was added to fractions containing His_6-n-*Nm*DsbD and His_6-c-*Nm*DsbD (0.2 and 0.4 mg TEV protease per 10 mg of protein, respectively) supplemented with 5 m*M* reduced dithiothreitol (DTT_{Red}) and samples were dialyzed overnight against 25 m*M* Tris pH 8.0, 150 m*M* NaCl. The samples were further purified using a 5 ml HisTrap FF column followed by size-exclusion chromatography (SEC) using a Superdex S-75 16/60 column (GE Healthcare) pre-equilibrated in 25 m*M* HEPES pH 6.7, 150 m*M* NaCl. The target proteins were oxidized using 1.7 m*M* copper phenanthrolene or reduced using 40 molar equivalents of reduced DTT and incubated for 1 h at 277 K. Oxidized and reduced proteins were buffer-exchanged into 25 m*M* HEPES pH 6.7, 50 m*M* NaCl and the same buffer supplemented with 1 m*M* EDTA using a 10 ml PD10 column (GE Healthcare) prior to crystallization experiments. The redox state of the *Nm*DsbD domains was confirmed by Ellman's assay (Evans & Ellman, 1959).

2.2. Small-angle X-ray scattering (SAXS) studies

SAXS data for n-*Nm*DsbD and c-*Nm*DsbD were collected on the SAXS-WAXS beamline at the Australian Synchrotron (Kirby *et al.*, 2013; Table 2). Serial dilutions of an ∼5 mg ml^{-1} stock were loaded into a 96-well plate. The estimated molecular mass was calculated using contrast and partial specific volumes determined from the protein sequences (Whitten *et al.*, 2008). The pair-distance distribution function [$p(r)$] was generated from the experimental data using *GNOM* (Svergun, 1992), from which $I(0)$, R_g and D_{max} were determined (Figs. 1*a* and 1*b*). The program *DAMMIN* (Svergun, 1999) was used to generate 16 molecular envelopes for each protein, which were averaged using the program *DAMAVER* (Volkov & Svergun, 2003), and the resolutions of the averaged structures were estimated using *SASRES* (Tuukkanen *et al.*, 2016). The experimental scattering data were compared with scattering curves calculated from the crystal structures of the corresponding domains from *E. coli* [n-*Ec*DsbD, PDB entry 1l6p (Goulding *et al.*, 2002), and c-*Ec*DsbD, PDB entry 1uc7 (Kim *et al.*, 2003)] using *CRYSOL* (Svergun *et al.*, 1995) (Fig. 1).

2.3. Crystallization

Initial high-throughput crystallization experiments were performed at 293 K either in-house using a Mosquito crystallization robot (TTP Labtech) or a Crystal Gryphon Liquid Handling System (Art Robbins Instruments) or at the CSIRO Collaborative Crystallisation Centre (http://www.csiro.au/C3), Melbourne, Australia. For n-*Nm*DsbD$_{Ox}$, c-*Nm*DsbD$_{Ox}$, n-*Nm*DsbD$_{Red}$ and c-*Nm*DsbD$_{Red}$, 96-well hanging-drop plates were prepared using 71, 44, 60 and 20–40 mg ml^{-1} protein solutions, respectively, and commercially available crystallization screens (Crystal Screen, Crystal Screen 2, PEG/Ion, PEG/Ion 2, Index and Salt RX from Hampton Research, PACT *premier* and JCSG-*plus* from Molecular Dimensions Ltd and Precipitant Synergy from Jena Bioscience) and an in-house malonate grid screen (pH 5–7 and 0.2–3.4 *M* malonate).

Initial crystallization experiments for the reduced proteins (n-*Nm*DsbD$_{Red}$ and c-*Nm*DsbD$_{Red}$) were performed using a Crystal Gryphon Liquid Handling System (Art Robbins Instruments). Crystallization experiments for n-*Nm*DsbD$_{Red}$ were set up with 60 mg ml^{-1} protein solution, whereas experiments for c-*Nm*DsbD$_{Red}$ were set up with both 20 and 40 mg ml^{-1} protein solutions. 96-well sitting-drop plates (200 nl protein solution and 200 nl reservoir solution equilibrated against 70 µl reservoir solution) were prepared using commercially available crystallization screens (PEG/Ion 1 and 2, Salt RX, Index, Crystal Screen and Crystal Screen 2 from Hampton Research and PACT *premier*, JCSG-*plus* and Morpheus from Molecular Dimensions Ltd).

All crystal-optimization experiments were carried out at 293 K in 24-well hanging-drop VDXm plates using 18 mm siliconized cover slips (Hampton Research), a reservoir volume of 500 µl and a drop size of 2 µl (1 µl protein and 1 µl reservoir solution).

Crystals of n-*Nm*DsbD$_{Ox}$ only grew in 20%(*w*/*v*) PEG 6000, 0.01 *M* zinc chloride, 0.1 *M* MES pH 6 (PACT *premier*). This condition was optimized by varying different components and diffraction-quality single hexagonal crystals (Figs. 2*a* and 2*c*) grew overnight using protein at 66 mg ml^{-1} in 18–20%(*w*/*v*) PEG 6000, 0.1 *M* MES pH 6.4, 0.02 *M* $ZnCl_2$.

Initial screening for n-*Nm*DsbD$_{Red}$ produced microcrystals in 2.5 *M* ammonium sulfate, 0.1 *M* Tris pH 8.5 (condition 1; from Salt RX), 0.1 *M* HEPES pH 7.5, 1.4 *M* sodium citrate tribasic dehydrate (condition 2; from Index), 5% Tacsimate pH 7.0, 0.1 *M* HEPES pH 7.0, 10%(*w*/*v*) PEG MME 5000 (condition 3; from Index), 0.1 *M* ammonium citrate tribasic pH 7.0, 12%(*w*/*v*) PEG 3350 (condition 4; from Index), 20%(*w*/*v*) PEG 3350, 0.2 *M* potassium nitrate (condition 5; from JCSG) and 0.1 *M* bis-tris propane pH 7.5, 20%(*w*/*v*) PEG 3350, 0.2 *M* sodium nitrate (condition 6; from PACT *premier*).

Optimization screens were prepared using protein at 30 and 60 mg ml^{-1}, and the best initial hits and small hexagonal diffraction-quality crystals (Figs. 2*b* and 2*d*) grew amongst salt crystals within 2 d in 2.5 *M* ammonium sulfate, 0.1 *M* Tris pH 9.1 with a protein concentration of 60 mg ml^{-1}.

Initial screening of c-*Nm*DsbD$_{Ox}$ yielded crystals in only one condition consisting of 5%(*w*/*v*) PEG 400, 2 *M* sodium citrate/citric acid pH 7.5 (Precipitant Synergy), and diffraction-quality crystals were obtained using protein at 42–38 mg ml^{-1} in 5%(*w*/*v*) PEG 400, 1.7–2.2 *M* citrate/citric acid pH 7.0–7.8.

Table 2
SAXS data-collection and analysis details.

	n-*Nm*DsbD	c-*Nm*DsbD
Data-collection parameters		
Instrument	SAXS-WAXS (Australian Synchrotron)	
Beam geometry	Point	
Wavelength (Å)	1.127	
Sample-to-detector distance (m)	1.480	
q-range (Å^{-1})	0.01–0.60	
Exposure time (s)	60 (30 × 2 s exposures)	
Protein concentration range† (mg ml^{-1})	∼0.3–5.0	
Temperature (K)	285	
Standard	Water	
Structural parameters		
$I(0)$ (cm^{-1}) (from Guinier)	0.00776 ± 0.00003	0.00997 ± 0.00002
R_g (Å) (from Guinier)	17.6 ± 0.2	15.3 ± 0.1
$I(0)$ (cm^{-1}) [from $p(r)$]	0.007688 ± 0.000012	0.009905 ± 0.000011
R_g (Å) [from $p(r)$]	17.3 ± 0.1	14.8 ± 0.1
D_{max} (Å)	57 ± 3	45 ± 3
Molecular-mass determination		
Protein concentration (mg ml^{-1})	0.74	1.12
Partial specific volume (cm^3 g^{-1})	0.73	0.73
Contrast, $\Delta\rho$ (10^{10} cm^{-2})	2.91	2.97
Molecular mass M_r [from $I(0)$]	13200 ± 1000	11800 ± 1000
Molecular mass M_r (expected)	13911	13358
Software employed		
Primary data reduction	*scatterBrain* (v.1.0)	
Data processing	*PRIMUS* (v.3.2) and *GNOM* (v.4.6)	
Ab initio modelling	*DAMMIN* (v.5.3)	
Validation and averaging	*DAMAVER* (v.2.8.0)	
Computation of model intensities	*CRYSOL* (v.2.8.3)	

† The R_g for n-*Nm*DsbD showed mild concentration dependence above a concentration of 1.0 mg ml^{-1}, decreasing from ∼17.5 Å at 0.37 mg ml^{-1} to ∼16 Å at 5.88 mg ml^{-1}. The 0.74 mg ml^{-1} data set was used for further analysis and modelling as it was deemed to be the highest concentration at which the effects of concentration were negligible. The change in R_g for c-*Nm*DsbD showed no obvious systematic trend in the concentration range measured. A concentration of 1.12 mg ml^{-1} was chosen for further analysis and modelling.

These thin spear-shaped crystals grew under a skin after between 4 and 8 d (Figs. 3*a* and 3*c*).

Initial screening of c-*Nm*DsbD$_{Red}$ yielded crystals in the following conditions: 0.2 *M* zinc acetate dehydrate, 0.1 *M* sodium cacodylate trihydrate pH 6.5, 18%(*w*/*v*) PEG 8000 (condition 1), 2.4 *M* sodium malonate pH 7 (condition 2), 0.1 *M* Tris–HCl pH 8.5, 2 *M* ammonium sulfate (condition 3; from Crystal Screen), 2 *M* ammonium sulfate (condition 4; from Crystal Screen) and 2.1 *M* DL-malic acid (condition 5; from JCSG-*plus*). Diffraction-quality crystals of c-*Nm*DsbD$_{Red}$ were obtained using protein at 30 mg ml^{-1} in 0.2 *M* zinc acetate dihydrate, 0.1 *M* sodium cacodylate trihydrate pH 7.5, 18%(*w*/*v*) PEG 8000. Clustered crystals grew in 3 d, or overnight with microseeding, and were subsequently manipulated to isolate single crystals for diffraction data collection (Figs. 3*b* and 3*d*).

All final crystallization conditions for the crystals used for data collection are described in Table 3.

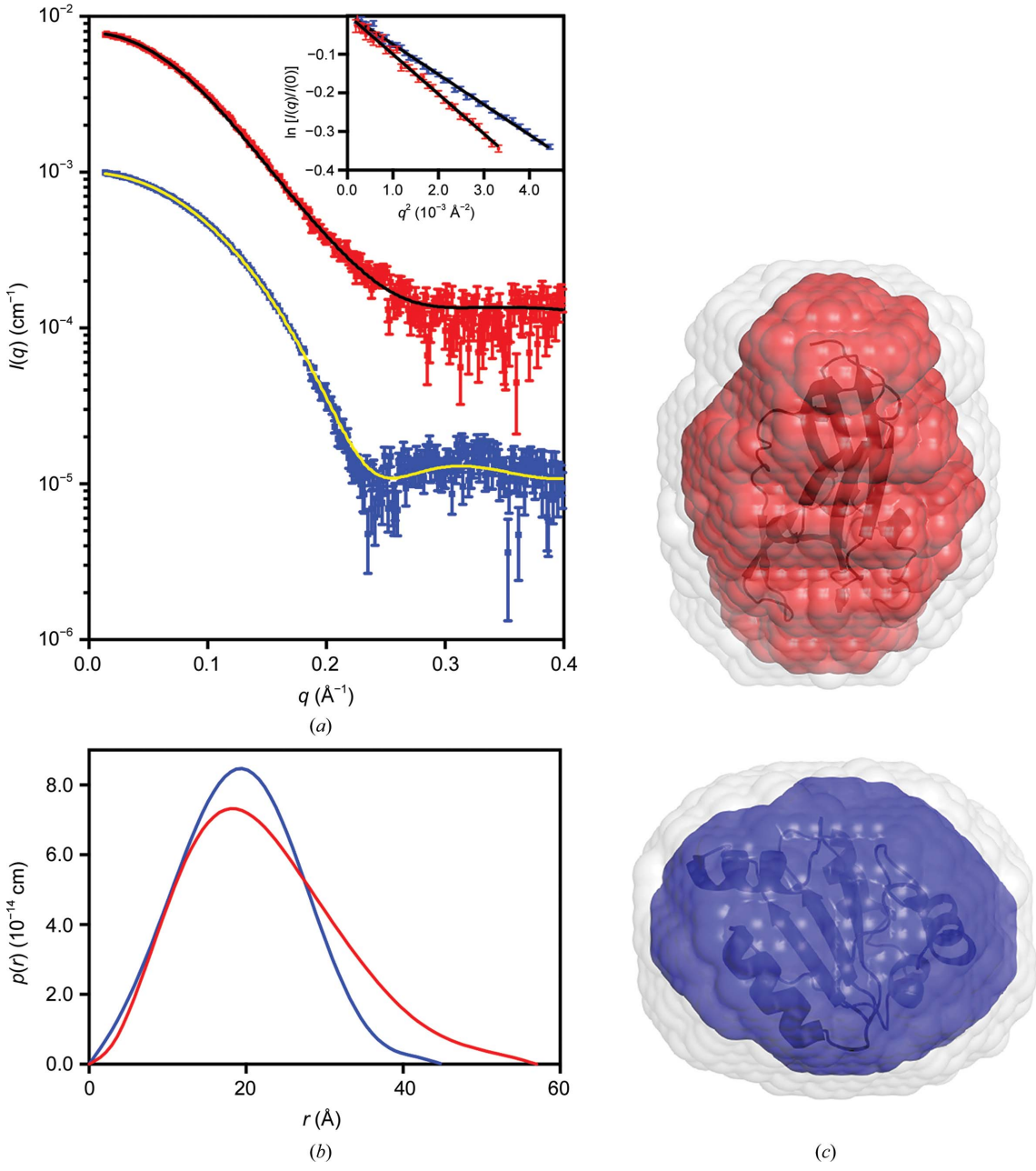

Figure 1
Small-angle X-ray scattering from n-*Nm*DsbD and c-*Nm*DsbD. (*a*) Measured scattering data for n-*Nm*DsbD (red) and c-*Nm*DsbD (blue; scaled by a factor of 0.1 for clarity). Overlaid are the calculated scattering curves for n-*Ec*DsbD (PDB entry 1l6p; black curve, $\chi^2 = 2.38$) and c-*Ec*DsbD (PDB entry 1uc7; yellow curve, $\chi^2 = 1.65$). Inset: Guinier plots of the scattering data. (*b*) The pair-distance distribution functions for n-*Nm*DsbD (red) and c-*Nm*DsbD (blue). (*c*) Probable domain shapes for n-*Nm*DsbD (SASBDB entry SASDCH7; red envelope, resolution = 19 ± 2 Å) and c-*Nm*DsbD (SASBDB entry SASDCJ7; blue envelope, resolution = 18 ± 2 Å) obtained from *ab intio* modelling against the scattering data. The crystal structures of n-*Ec*DsbD (PDB entry 1l6p) and c-*Ec*DsbD (PDB entry 1uc7) are shown as cartoons. The grey envelopes represent the total volume encompassed by the 16 aligned models for n-*Nm*DsbD ($\chi^2 = 1.90 \pm 0.01$) and c-*Nm*DsbD ($\chi^2 = 1.60 \pm 0.01$).

2.4. X-ray diffraction data measurements

For diffraction data measurements, n-*Nm*DsbD$_{Ox}$, c-*Nm*DsbD$_{Ox}$ and n-*Nm*DsbD$_{Red}$ crystals were cryoprotected by soaking them for 2 min in mother liquor supplemented with 20% glycerol, PEG 400 and glycerol, respectively. c-*Nm*DsbD$_{Red}$ crystals were cryocooled in reservoir solution. X-ray diffraction data were collected at 100 K on the micro-focus beamline (MX2) at the Australian Synchrotron using an ADSC Quantum 315r detector. Diffraction data were collected over a total angular rotation of 180° for both the n-*Nm*DsbD$_{Ox}$ and n-*Nm*DsbD$_{Red}$ crystals, with an oscillation angle of 1° and an exposure time of 1 s. A total of 180° of diffraction images were also collected for the c-*Nm*DsbD$_{Ox}$ crystal, with an oscillation angle of 0.5° and an exposure time of 1 s. For the c-*Nm*DsbD$_{Red}$ crystal the oscillation range per image was 1° over a total angular rotation of 200°, with an exposure time of 0.5 s. Diffraction data were indexed, integrated and scaled using *HKL*-2000 (Otwinowski & Minor, 1997) for the n-*Nm*DsbD$_{Ox}$ and c-*Nm*DsbD$_{Ox}$ data sets, and using *iMosflm* (Battye *et al.*, 2011) and *AIMLESS* from the *CCP*4 suite (Winn *et al.*, 2011) for the n-*Nm*DsbD$_{Red}$ and c-*Nm*DsbD$_{Red}$ data sets.

3. Results and discussion

The two periplasmic domains of the thiol-disulfide reductase DsbD from *N. meningitidis*, n-*Nm*DsbD and c-*Nm*DsbD, were recombinantly expressed in *E. coli* and purified to homogeneity using three chromatographic steps (affinity, reverse affinity and size-exclusion chromatography) for crystallization trials.

We first analyzed n-*Nm*DsbD and c-*Nm*DsbD using SAXS not only to determine the quality of the recombinant proteins in solution but also to obtain low-resolution information on

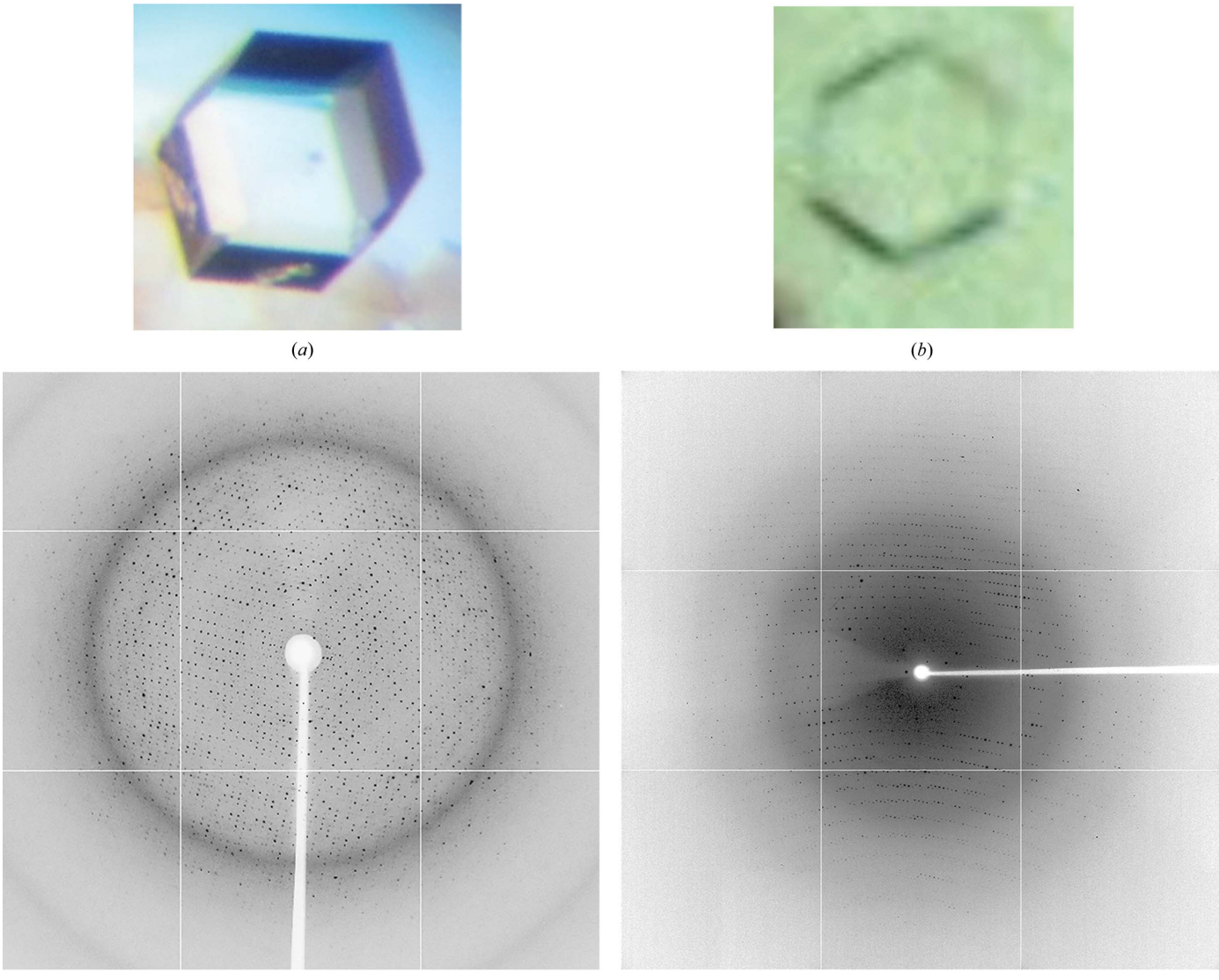

Figure 2
Crystals and diffraction patterns for n-*Nm*DsbD (this domain shares 30% sequence identity with n-*Ec*DsbD; PDB entry 1l6p). (*a*) n-*Nm*DsbD$_{Ox}$ crystals with approximate dimensions of 0.30 × 0.25 × 0.40 mm. (*b*) n-*Nm*DsbD$_{Red}$ crystals with approximate dimensions of 0.1 × 0.05 × 0.1 mm. Diffraction images are shown for (*c*) n-*Nm*DsbD$_{Ox}$ and (*d*) n-*Nm*DsbD$_{Red}$ crystals.

the shape and conformation of these domains (Fig. 1). The SAXS data displayed a low experimental noise level, with a linear Guinier plot consistent with a homogeneous, monodisperse solution of both *Nm*DsbD domains. The molecular weights of n-*Nm*DsbD and c-*Nm*DsbD estimated from extrapolation to $I(0)$ were 13.2 and 11.9 kDa, respectively. *Ab initio* modelling was employed to determine the low-resolution structure of both domains. 16 low-resolution

Table 3
Crystallization.

	n-*Nm*DsbD$_{Ox}$	n-*Nm*DsbD$_{Red}$	c-*Nm*DsbD$_{Ox}$	c-*Nm*DsbD$_{Red}$
Method	Hanging drop	Hanging drop	Hanging drop	Hanging drop
Plate type	VDXm plates	VDXm plates	VDXm plates	VDXm plates
Temperature (K)	291	291	291	291
Protein concentration (mg ml^{-1})	66	61	40	30
Buffer composition of protein solution	0.025 *M* HEPES, 0.05 *M* NaCl pH 6.7	0.025 *M* HEPES, 0.05 *M* NaCl pH 6.7	0.025 *M* HEPES, 0.05 *M* NaCl pH 6.7	0.025 *M* HEPES, 0.05 *M* NaCl pH 6.7
Composition of reservoir solution	18–20%(*w*/*v*) PEG 6000, 0.1 *M* MES pH 6.4, 0.020 *M* $ZnCl_2$	2.5 *M* ammonium sulfate, 0.1 *M* Tris pH 9.1	5%(*w*/*v*) PEG 400, 1.7–2.2 *M* citrate/citric acid pH 7.0–7.8	0.2 *M* zinc acetate dehydrate, 0.1 *M* sodium cacodylate trihydrate pH 7.5, 18%(*w*/*v*) PEG 8000
Volume and ratio of drop	2 µl, 1:1	2 µl, 1:1	2 µl, 1:1	2 µl, 1:1
Volume of reservoir (µl)	500	500	500	500

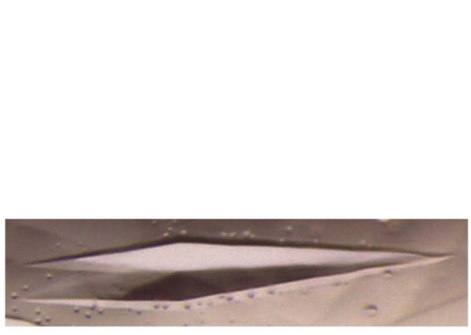

(*a*)

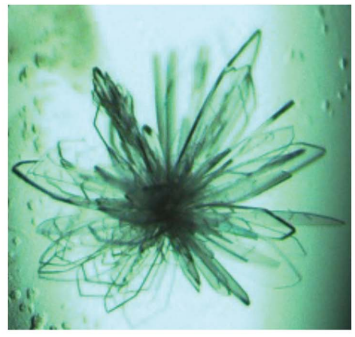

(*b*)

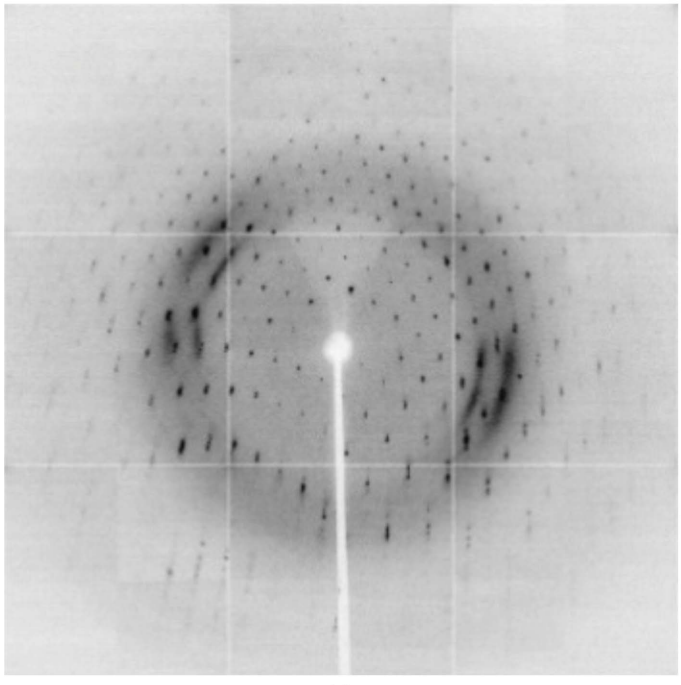

(*c*)

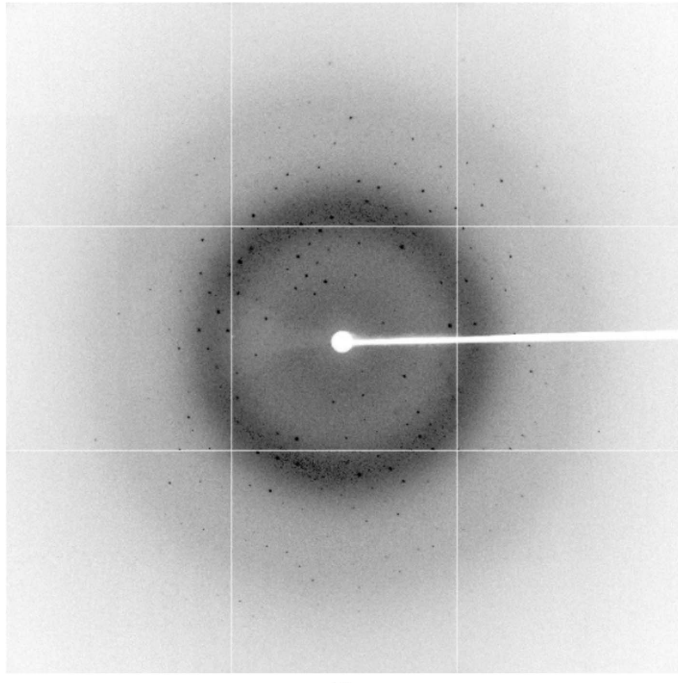

(*d*)

Figure 3
Crystals and diffraction patterns for c-*Nm*DsbD (this domain shares 38% sequence identity with c-*Ec*DsbD; PDB entry 2fwe). (*a*) c-*Nm*DsbD$_{Ox}$ crystals with approximate dimensions of 0.10 × 0.05 × 0.50 mm. (*b*) c-*Nm*DsbD$_{Red}$ crystal cluster. Diffraction images are shown for (*c*) c-*Nm*DsbD$_{Ox}$ and (*d*) c-*Nm*DsbD$_{Red}$ crystals.

Table 4
Data collection and processing.

Values in parentheses are for the highest resolution shell.

	n-*Nm*DsbD$_{Ox}$	n-*Nm*DsbD$_{Red}$	c-*Nm*DsbD$_{Ox}$	c-*Nm*DsbD$_{Red}$
Diffraction source	Australian Synchrotron	Australian Synchrotron	Australian Synchrotron	Australian Synchrotron
Wavelength (Å)	0.9537	0.9537	0.9537	0.9537
Temperature (K)	100	100	100	100
Detector	ADSC Quantum 315r	ADSC Quantum 315r	ADSC Quantum 315r	ADSC Quantum 315r
Rotation range per image (°)	1	1	0.5	1
Total rotation range (°)	180	180	180	200
Exposure time per image (s)	1	1	1	0.5
Space group	$P2_13$	$P321$	$P4_1$	$P12_11$
a, b, c (Å)	147.64, 147.64, 147.64	116.98, 116.98, 45.79	35.80, 35.80, 188.74	43.25, 28.06, 45.80
α, β, γ (°)	90, 90, 90	90, 90, 120	90, 90, 90	90, 101, 90
Predicted solvent content (%)	61.50	62.65	46.37	41.17
Resolution range (Å)	50.00–2.60 (2.69–2.60)	45.79–1.60 (1.69–1.60)	50.00–2.30 (2.38–2.30)	42.46–1.70 (1.79–1.70)
Total No. of reflections	432319	504136	131158	46022
No. of unique reflections	32934	47439	10483	12150
Completeness (%)	99.9 (100)	100 (100)	99.8 (100)	99.8 (99.9)
Redundancy (multiplicity)	13.1 (12.6)	10.6 (10.5)	12.5 (12.7)	3.8 (3.9)
$\langle I/\sigma(I)\rangle$	14.0 (4.6)	11.4 (1.8)	20.4 (6.3)	7.5 (2.2)
$R_{r.i.m.}$†	0.09 (0.365)	0.08 (1.06)	0.07 (0.281)	0.067 (0.357)
$R_{p.i.m.}$	0.051 (0.213)	0.046 (0.594)	0.039 (0.155)	0.059 (0.306)

† Calculated by multiplying $R_{merge} = \sum_{hkl}\sum_i |I_i(hkl) - \langle I(hkl)\rangle| / \sum_{hkl}\sum_i I_i(hkl)$, where $I(hkl)$ is the intensity of individual reflections, by the factor $[N/(N-1)]^{1/2}$, where N is the data multiplicity.

models were generated and subsequently aligned, averaged and filtered to produce the probable shape of the protein (Fig. 1*c*). The agreement between the crystal structures of the n-*Ec*DsbD and c-*Ec*DsbD domains and the red and blue envelopes provides convincing evidence that the n-*Nm*DsbD and c-*Nm*DsbD domains adopt similar three-dimensional structures in solution to their *E. coli* counterparts.

Despite the only difference between n-*Nm*DsbD$_{Ox}$ and n-*Nm*DsbD$_{Red}$ or c-*Nm*DsbD$_{Ox}$ and c-*Nm*DsbD$_{Red}$ being the presence or absence of a disulfide bond, the domains crystallized in different conditions in their two redox forms. Single crystals of n-*Nm*DsbD$_{Ox}$ grew in 18–20%(*w*/*v*) PEG 6000, 100 m*M* MES pH 6.4, 20 m*M* $ZnCl_2$. n-*Nm*DsbD$_{Red}$ crystals were obtained in 2.5 *M* ammonium sulfate, 0.1 *M* Tris pH 9.1. c-*Nm*DsbD$_{Ox}$ crystallized in 5%(*w*/*v*) PEG 400, 1.7–2.2 *M* citrate/citric acid pH 7.0–7.8 and crystals of c-*Nm*DsbD$_{Red}$ grew in 0.2 *M* zinc acetate dehydrate, 0.1 *M* sodium cacodylate trihydrate pH 7.5, 18%(*w*/*v*) PEG 8000 (Figs. 2 and 3). The n-*Nm*DsbD$_{Ox}$, n-*Nm*DsbD$_{red}$, c-*Nm*DsbD$_{Ox}$ and c-*Nm*DsbD$_{Red}$ crystals diffracted to resolutions of 2.3, 1.6, 2.3 and 1.7 Å and belonged to space groups $P2_13$, $P321$, $P4_1$ and $P12_11$, respectively. Assuming that the n-*Nm*DsbD$_{Ox}$, n-*Nm*DsbD$_{Red}$, c-*Nm*DsbD$_{Ox}$ and c-*Nm*DsbD$_{Red}$ crystals contain six, two, two and one molecules per asymmetric unit, respectively, their respective Matthews coefficients (V_M) are 3.19, 3.29, 2.29 and 2.09 Å^3 Da^{-1} and their corresponding solvent contents are 61.50, 62.65, 46.37 and 41.17%, respectively (Matthews, 1968). Diffraction data statistics are shown in Table 4. Further studies are in progress to elucidate the structure and mode of action of these catalytic domains in *Nm*DsbD.

Acknowledgements

This research was undertaken on the MX and SAXS-WAXS beamlines at the Australian Synchrotron, Victoria, Australia. We acknowledge the use of The University of Queensland Remote Operated Crystallization X-ray Facility (UQROCX), Brisbane, Australia, the CSIRO Collaborative Crystallisation Centre (http://www.csiro.au/C3), Melbourne, Australia and the La Trobe Comprehensive Proteomics Platform, Melbourne, Australia.

Funding information

This work was supported by an Australian Research Council (ARC) project grant (DP150102287), a British Society for Antimicrobial Chemotherapy (BSAC) project grant and a National Health and Medical Research Council (NHMRC) Project Grant (APP1099151). BH is supported by an ARC Future Fellowship (FT130100580). RS is supported by a Research Training Program (RTP) Scholarship. CMK was supported by the National Health and Medical Research Council (APP546003).

References

Arts, I. S., Gennaris, A. & Collet, J.-F. (2015). *FEBS Lett.* **589**, 1559–1568.
Bardwell, J. C., Lee, J. O., Jander, G., Martin, N., Belin, D. & Beckwith, J. (1993). *Proc. Natl Acad. Sci. USA*, **90**, 1038–1042.
Battye, T. G. G., Kontogiannis, L., Johnson, O., Powell, H. R. & Leslie, A. G. W. (2011). *Acta Cryst.* D**67**, 271–281.
Cabrita, L. D., Gilis, D., Robertson, A. L., Dehouck, Y., Rooman, M. & Bottomley, S. P. (2007). *Protein Sci.* **16**, 2360–2367.
Cho, S.-H. & Beckwith, J. (2009). *J. Biol. Chem.* **284**, 11416–11424.
Cho, S.-H. & Collet, J.-F. (2013). *Antioxid. Redox Signal.* **18**, 1690–1698.
Cho, S.-H., Porat, A., Ye, J. & Beckwith, J. (2007). *EMBO J.* **26**, 3509–3520.
Depuydt, M., Leonard, S. E., Vertommen, D., Denoncin, K., Morsomme, P., Wahni, K., Messens, J., Carroll, K. S. & Collet, J.-F. (2009). *Science*, **326**, 1109–1111.
Depuydt, M., Messens, J. & Collet, J.-F. (2011). *Antioxid. Redox Signal.* **15**, 49–66.

Eschenfeldt, W. H., Lucy, S., Millard, C. S., Joachimiak, A. & Mark, I. D. (2009). *Methods Mol. Biol.* **498**, 105–115.
Evans, J. C. & Ellman, G. L. (1959). *Biochim. Biophys. Acta*, **33**, 574–576.
Goulding, C. W., Sawaya, M. R., Parseghian, A., Lim, V., Eisenberg, D. & Missiakas, D. (2002). *Biochemistry*, **41**, 6920–6927.
Heras, B., Kurz, M., Shouldice, S. R. & Martin, J. L. (2007). *Curr. Opin. Struct. Biol.* **17**, 691–698.
Heras, B., Shouldice, S. R., Totsika, M., Scanlon, M. J., Schembri, M. A. & Martin, J. L. (2009). *Nature Rev. Microbiol.* **7**, 215–225.
Kadokura, H. & Beckwith, J. (2010). *Antioxid. Redox Signal.* **13**, 1231–1246.
Kamitani, S., Akiyama, Y. & Ito, K. (1992). *EMBO J.* **11**, 57–62.
Katzen, F. & Beckwith, J. (2000). *Cell*, **103**, 769–779.
Katzen, F., Deshmukh, M., Daldal, F. & Beckwith, J. (2002). *EMBO J.* **21**, 3960–3969.
Kim, J. H., Kim, S. J., Jeong, D. G., Son, J. H. & Ryu, S. E. (2003). *FEBS Lett.* **543**, 164–169.
Kirby, N. M., Mudie, S. T., Hawley, A. M., Cookson, D. J., Mertens, H. D. T., Cowieson, N. & Samardzic-Boban, V. (2013). *J. Appl. Cryst.* **46**, 1670–1680.
Kumar, P., Sannigrahi, S., Scoullar, J., Kahler, C. M. & Tzeng, Y.-L. (2011). *Mol. Microbiol.* **79**, 1557–1573.
Matthews, B. W. (1968). *J. Mol. Biol.* **33**, 491–497.
Missiakas, D., Georgopoulos, C. & Raina, S. (1993). *Proc. Natl Acad. Sci. USA*, **90**, 7084–7088.
Missiakas, D., Georgopoulos, C. & Raina, S. (1994). *EMBO J.* **13**, 2013–2020.
Missiakas, D., Schwager, F. & Raina, S. (1995). *EMBO J.* **14**, 3415–3424.
Otwinowski, Z. & Minor, W. (1997). *Methods Enzymol.* **276**, 307–326.
Rietsch, A., Belin, D., Martin, N. & Beckwith, J. (1996). *Proc. Natl Acad. Sci. USA*, **93**, 13048–13053.
Rietsch, A., Bessette, P., Georgiou, G. & Beckwith, J. (1997). *J. Bacteriol.* **179**, 6602–6608.
Rozhkova, A., Stirnimann, C. U., Frei, P., Grauschopf, U., Brunisholz, R., Grütter, M. G., Capitani, G. & Glockshuber, R. (2004). *EMBO J.* **23**, 1709–1719.
Smith, R. P., Paxman, J. J., Scanlon, M. J. & Heras, B. (2016). *Molecules*, **21**, 811.
Stewart, E. J., Katzen, F. & Beckwith, J. (1999). *EMBO J.* **18**, 5963–5971.
Stirnimann, C. U., Rozhkova, A., Grauschopf, U., Grütter, M. G., Glockshuber, R. & Capitani, G. (2005). *Structure*, **13**, 985–993.
Studier, F. W. (2005). *Protein Expr. Purif.* **41**, 207–234.
Svergun, D. I. (1992). *J. Appl. Cryst.* **25**, 495–503.
Svergun, D. I. (1999). *Biophys. J.* **76**, 2879–2886.
Svergun, D., Barberato, C. & Koch, M. H. J. (1995). *J. Appl. Cryst.* **28**, 768–773.
Tuukkanen, A. T., Kleywegt, G. J. & Svergun, D. I. (2016). *IUCrJ*, **3**, 440–447.
Volkov, V. V. & Svergun, D. I. (2003). *J. Appl. Cryst.* **36**, 860–864.
Whitten, A. E., Cai, S. & Trewhella, J. (2008). *J. Appl. Cryst.* **41**, 222–226.
Winn, M. D. *et al.* (2011). *Acta Cryst.* D**67**, 235–242.